



# Photocatalytic cyclization of nitrogen-centered radicals with carbon nitride through promoting substrate/catalyst interaction

Received: 20 May 2022

Accepted: 9 August 2022

Published online: 20 August 2022



Mingcheng Yang<sup>1</sup>, Ronghong Lian<sup>1</sup>, Xirui Zhang<sup>1</sup>, Chong Wang<sup>1</sup>,  
Jiajia Cheng<sup>1,2</sup>✉ & Xinchun Wang<sup>1,2</sup>✉

The use of metal-free carbon nitride and light to drive catalytic transformations constitutes a sustainable strategy for organic synthesis. At the moment, enhancing the intrinsic activity of CN catalysts by tuning the interfacial coupling between catalyst and substrate remains challenging. Herein, we demonstrate that urea-derived carbon nitride catalysts with the abundant  $-NH_2$  groups and the relative positive charged surface could effectively complex with the deprotonated anionic intermediate to improve the adsorption of organic reactants on the catalyst surface. The decreased oxidation potential and upshift in its highest occupied molecular orbital position make the electron abstraction kinetics by the catalyst more energetically favorable. The prepared catalyst is thus utilized for the photocatalytic cyclization of nitrogen-centered radicals for the synthesis of diverse pharmaceutical-related compounds (33 examples) with high activity and reusability, which shows competent performance to the homogeneous catalysts.

Five-membered heterocyclics, such as the dihydropyrazole moiety as well as their unsaturated counterpart pyrazoles, are extensively found in pharmacologically active molecules, agrochemicals, natural products, and synthetic ligands<sup>1,2</sup>. The synthetic approaches towards the aza-heterocycles through photocatalytic intramolecular addition of nitrogen-centered radicals hold several advantages<sup>3–5</sup>. Nonetheless, due to the high bond dissociation free energies (BDFEs) of most N-H bonds (typically > 100 kcal/mol)<sup>6</sup>, giving rise to the nitrogen-centered radicals directly from N-H bonds meets several challenges<sup>7,8</sup>. Irradiating by the proton-coupled electron transfer (PCET) in the natural photosynthesis process<sup>9</sup>, an oxidative deprotonation electron transfer strategy combining base and photocatalyst has been developed<sup>10,11</sup>. Acridinium salts, as well as transition metal complexes based on ruthenium and iridium, have been shown to be good photocatalysts for preparing the dihydropyrazole frameworks<sup>12–15</sup>. Regardless of the advances made in the field of homogeneous catalysts, many issues

remain regarding costs, catalyst recovery, stability, and particularly metal leaching<sup>16–18</sup>. As a result, the development of efficient and selective strategies for metal-free heterogeneous photocatalytic heterocycle synthesis is still highly desirable.

Tailoring the interfacial interaction between semiconductor photocatalyst and the substrate is considered an important approach in the pursuit of advanced heterogeneous catalysis. The surface properties of the heterogeneous catalyst are crucial because they affect both the substrate-catalyst interaction and the mobility of the charge carriers<sup>19–21</sup>. The use of surface properties in heterogeneous catalysts also offers considerable opportunities to facilitate selective organic reactions through modulation of the reaction kinetics. Several important industrial transformations are catalyzed or promoted via the incorporation of acid and base surface sites of catalysts, such as oil cracking, alkylation, and isomerization<sup>22,23</sup>. The electron density of the metal nanoparticle

<sup>1</sup>State Key Laboratory of Photocatalysis on Energy and Environment, College of Chemistry, Fuzhou University, Fuzhou 350116, China. <sup>2</sup>Qingyuan Innovation Laboratory, Quanzhou 362801, China. ✉ e-mail: [jjcheng@fzu.edu.cn](mailto:jjcheng@fzu.edu.cn); [xcwang@fzu.edu.cn](mailto:xcwang@fzu.edu.cn)

and consequently the adsorption of organic molecules on their surface could also be effectively modified through the interaction between metal catalyst and support. For instance, adjustment of the catalyst surface basicity may improve the photocatalytic performance in the oxidation of the primary alcohols to aldehydes<sup>24</sup>, while the effective promotion of hydrogen transfer by basic sites on bismuth oxybromide can enhance solar-driven reduction and oxidation reactions<sup>25</sup>.

Benefitting from the high thermal and chemical stability, superior photovoltaic characteristics, and unique electronic structure, polymeric carbon nitride (CN) materials have been demonstrated to be efficient photocatalysts for a variety of catalytic reactions<sup>26–28</sup>. The CN materials possess distinctive surface properties such as functional Brønsted acid and base sites<sup>29–31</sup>, which can endow the system with a catalytic activity that is absent in the pristine materials<sup>32,33</sup>. However, most of the current CN-photocatalysts for selective organic synthesis have concentrated on thermodynamic processes. Enhancing the intrinsic activity by tuning the interfacial interaction between catalyst and substrate remains challenging<sup>34–36</sup>. As a result, we propose that the redox potentials of critical organic reactants, specifically the deprotonated anionic intermediate in this case, can be altered by surface complexation with the CN catalyst, which can then be used in conjunction with photocatalyst to enable demanding conversions under mild conditions.

We report herein the general heterogeneous photocatalytic strategy for the synthesis of functionalized dihydropyrazoles from N-H hydrazone<sup>37</sup> over CN (Fig. 1). Three CN samples (g-CN-U, g-CN-DCDA, and K-PHI) with different surface properties were prepared<sup>38,39</sup>. It is observed that urea-derived carbon nitride (g-CN-U) with abundant  $\text{-NH}_2$  groups and relative positive surface could effectively complex with the in-situ generated anionic intermediate to improve the adsorption and activation of the key species on the catalyst surface. Moreover, the upshift in its highest occupied molecular orbital (HOMO) position makes the electron abstraction more energetically favorable. Therefore, the highly selective oxidation of the hydrazone N-H bond to nitrogen-centered radical could be achieved over g-CN-U, whereas g-CN-DCDA and K-PHI showcased inferior activity<sup>40</sup>. This approach would open up the possibility of utilizing surface complexation between the catalysts and vital reaction intermediates to promote a broad range of photoredox reactions.

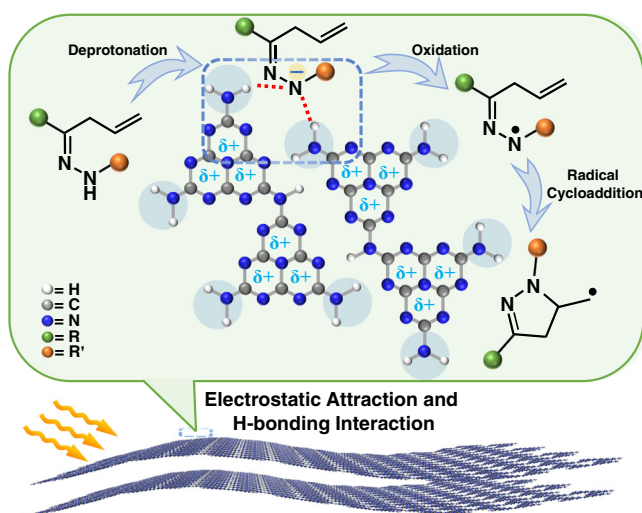


**Fig. 1 | Interface assisted catalytic cyclization of nitrogen-centered radicals over carbon nitride.** Photocatalytic oxidative cyclization of hydrazones through promoting substrate/catalyst interaction.

## Results and discussion

### Photocatalytic cyclization of nitrogen-centered radicals over carbon nitride

For comparison, three CN samples with distinct surface properties were prepared. The g-CN-U photocatalyst, which possesses a positive surface<sup>38</sup>, is synthesized by pyrolysis of urea at 550 °C. The g-CN-DCDA sample with fewer  $\text{-NH}_2$  groups and different surface properties is synthesized from dicyandiamide (DCDA). The K-PHI catalyst, which is derived from preheated melamine after KCl/LiCl molten salt treatment is chosen as another comparative photocatalyst owing to its negatively charged nitrogen atoms<sup>41,42</sup>. Powder X-ray diffraction (PXRD) analysis confirms the crystalline structure and layered-stacking mode of the photocatalysts (Fig. 2a). The solid-state  $^{13}\text{C}$  NMR (CP-MAS) of the samples all exhibited two intensive peaks at 160 and 168 ppm, respectively, associated with the chemical shifts of the C(i) and C(e) atoms in the heptazine units. This result suggested a similar heptazine-based structure of the prepared samples (Supplementary Fig. 1). In the Fourier transform infrared (FT-IR) spectroscopy, the characteristic peaks associated with the heptazine units could be observed, suggesting the identical framework of the samples. Notably, the intensity of the peak located at around  $3250\text{ cm}^{-1}$  of g-CN-U is stronger than g-CN-DCDA and K-PHI, indicating the existence of abundant  $\text{NH}_2$  groups on the g-CN-U surface. Whereas, K-PHI shows an additional  $1000\text{ cm}^{-1}$  peak corresponding to the N-K bond and a  $2180\text{ cm}^{-1}$  peak to the cyanamide groups (Fig. 2b). The observed intensity at  $2180\text{ cm}^{-1}$  in the Raman spectra of K-PHI may also correlate with the cyanamide-functionality vibrational frequency (Fig. 2c). Elemental analysis (EA) results showed that the samples all contained C, N, H elements with a similar C/N ratio (Supplementary Table 1), whereas the H element of g-CN-U is the largest, consistent with the richness of  $\text{NH}_2$  groups from the IR results. Inductively coupled plasma mass spectrometry atomic emission spectroscopy (ICP-AES) analysis revealed that except for a small amount of K ions existed in the K-PHI sample, none of the Co, Ni, Cu, Ru, or Pd atoms were present in the g-CN-U, g-CN-DCDA and K-PHI samples (Supplementary Table 2). The robustness of the photocatalysts could be demonstrated by the thermogravimetric analysis (TGA), which would not decompose until 400 °C (Supplementary Fig. 2).

The photocatalytic reaction was commenced with hydrazone **1a** as the model substrate, the synthesized CN samples as the photocatalysts, and NaOH as the base under an  $\text{N}_2$  atmosphere. The cyclization cannot proceed via heating conditions due to the high BDFE of the N-H bonds (Supplementary Fig. 3). No product was obtained without the photocatalyst either (Fig. 2d). Basically, a semiconductor with the valence-band edge lower than the nitrogen-centered anion/radical redox potential may photocatalyze the transformation. However, of all the examined CN catalysts, dihydropyrazole was formed as a major product only over g-CN-U. The major byproduct was  $\beta,\gamma$ -unsaturated ketone derived from hydrolysis of hydrazone and desulfonation derivative of the dihydropyrazole product (Supplementary Fig. 4). g-CN-DCDA led to a lower yield, whilst the K-PHI catalyst shows the least catalytic efficiency (Fig. 2d). Only a trace amount of product was obtained without base (Supplementary Fig. 5a). Other bases such as  $\text{Na}_2\text{CO}_3$ ,  $\text{NaHCO}_3$ , or  $\text{Et}_3\text{N}$  also delivered the product, albeit in a lower yield. The optimal reaction system was performed in  $\text{CHCl}_3$  (Supplementary Fig. 5b), indicating the possible involvement of the hydrogen atom transfer (HAT) process<sup>43</sup>. Examination of light wavelength showed that the reaction could proceed in extended light wavelength (Supplementary Fig. 5c). In comparison to other commonly used heterogeneous photocatalysts, such as  $\text{TiO}_2$ , CdS, BCN, or  $\text{ZnIn}_2\text{S}_4$ , g-CN-U showed the best performance (Supplementary Fig. 5d). Consequently, the desired five-membered heterocycle could be produced in 80% isolated yield over metal-free g-CN-U photocatalyst, which is comparable to that of the homogeneous catalytic systems (Supplementary Table 3).

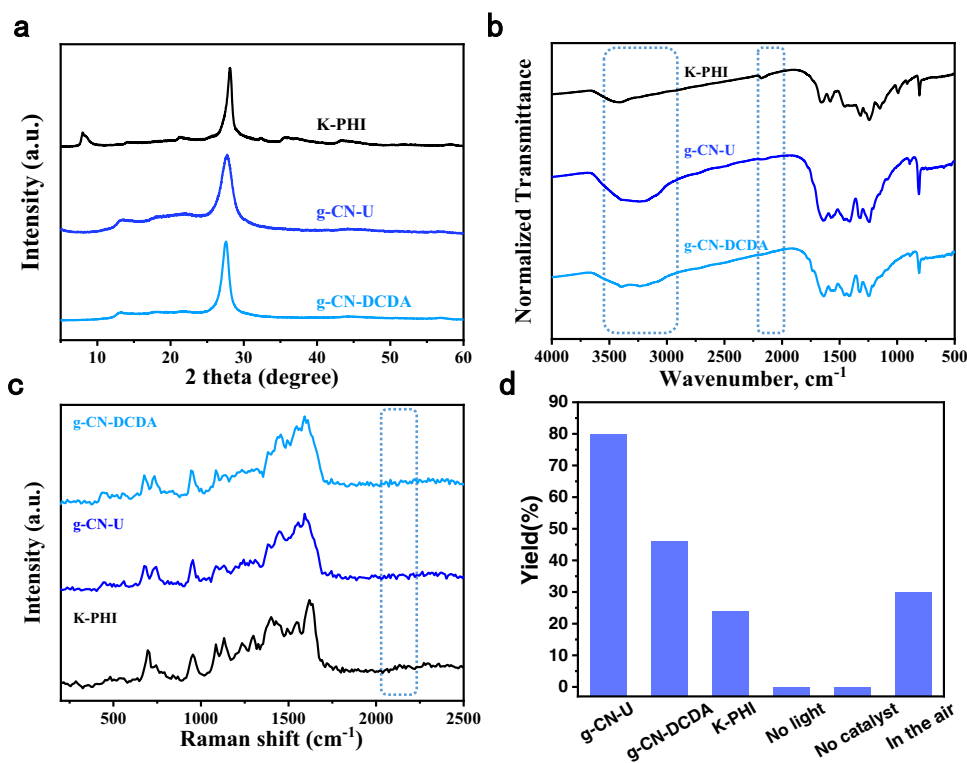


**Fig. 2 | Structural characterizations.** **a** PXRD result of g-CN-U, g-CN-DCDA, K-PHI. **b** FT-IR spectra of g-CN-U, g-CN-DCDA, K-PHI. **c** Raman spectra of g-CN-U, g-CN-DCDA, K-PHI. **d** Photocatalytic activities under the different photocatalysts: 1a

(0.1 mmol), NaOH (1.5 equiv.), catalyst (5 mg),  $\text{CHCl}_3$  (2 mL), 3 W 420 nm LED, under  $\text{N}_2$  at room temperature for 8 h. Yields determined by  $^1\text{H}$  NMR using benzyl ether as an internal standard.

### Mechanism study

As observed from  $^1\text{H}$  NMR, addition of NaOH to the hydrazone solution led to the full deprotonation and the formation of a nitrogen-centered anion swiftly (Supplementary Fig. 6). The oxidation potential of the anion/radical (+0.76 V vs. NHE) by cyclic voltammetry (Supplementary Fig. 7) is substantially less than that of  $\text{NH}/\text{NH}^+$  (+1.0 V vs. NHE) (Supplementary Fig. 8). The inclusion of a radical scavenger (TEMPO, BQ, or DMPO) significantly suppressed the product formation (Fig. 3a). The light on-off switching experiments excluded a radical chain process (Fig. 3b). In situ-electron spin resonance (ESR) spectroscopy revealed a carbon-centered radical species (Fig. 3c). The isolation of TEMPO-trapping product **10** in excellent yield confirmed this hypothesis (Fig. 3e and Supplementary Fig. 9). The reaction was then conducted in  $\text{CDCl}_3$  (Fig. 3f and Supplementary Fig. 10) and a 1:1 ratio of **2 h** and **2 h'** in 33% combined yield was observed, confirming the origin of the partial hydrogen source from  $\text{CHCl}_3$ . A zero-order kinetic profile indicated that the rate-determining step occurs as a result of adsorption of the reactive species at the g-CN-U surface (Fig. 3d)<sup>44</sup>.

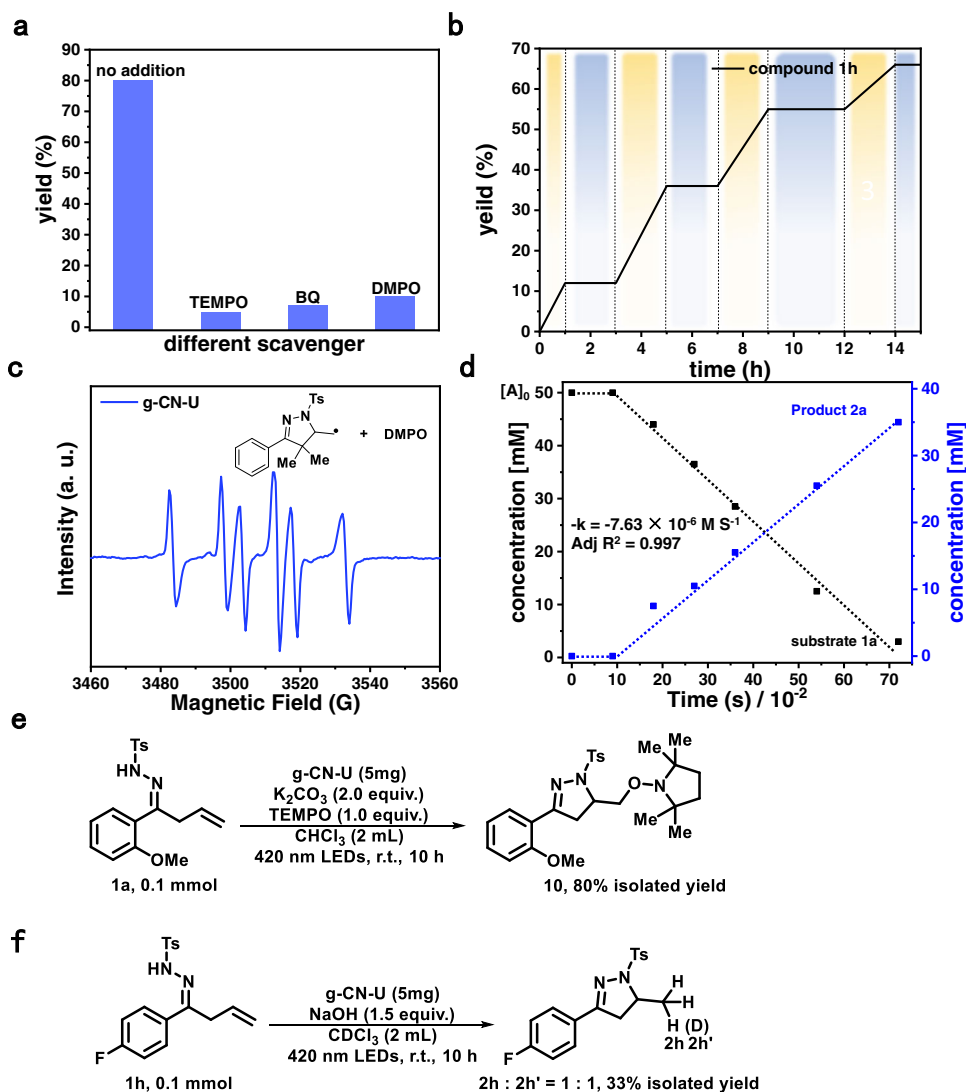
Based on our results and previous reports<sup>11,12</sup>, this reaction possibly proceeds through the following reaction pathway (Supplementary Fig. 11). Deprotonation of hydrazone first occurs to generate the anionic intermediate **Int A**. The single-electron oxidation by the light-excited valence band (VB) hole of the photocatalyst took place to deliver the nitrogen-centered radical **Int B**. A 5-exo-trig cyclization of **Int B** furnished the carbon-centered radical **Int C**. Due to the high instability of the carbon anion (e.g., *t*-butyl radical,  $E_{1/2}^{\text{red}} = -2.54$  V vs SCE in MeCN)<sup>45</sup>, the reduction of **Int C** to afford the carbon anion may not be feasible. Therefore, HAT from  $\text{CHCl}_3$  ( $\text{CHCl}_3$  exhibited a relatively weak C-H BDE of 93 kJ/mol)<sup>46</sup> contributed to product **2** and trichloromethyl radical. The formed trichloromethyl radical (Supplementary Fig. 12) could be readily reduced by the conduction band (CB) electron to give trichloromethanide anion (Supplementary

Fig. 13) and finally obtained one proton from the environment to complete the catalytic cycle<sup>47</sup>.

### Interface-assisted substrate-catalyst coupling to activate the key deprotonated hydrazone intermediate and promote the reaction

As shown in the UV-vis absorption features (Supplementary Fig. 14), g-CN-U both exhibited one blue-shift and less intensified light absorption with a bandgap of 2.92 eV (Supplementary Fig. 15). The VB maximum of g-CN-U exists at +1.76 V, similar to g-CN-DCDA, while K-PHI exhibit a stronger oxidation capability at +1.90 V (Supplementary Fig. 17). According to the results of photoluminescence (PL) spectrum (Supplementary Fig. 18), photocurrent response and electrochemical impedance spectroscopy (EIS) (Supplementary Fig. 19), the charge generation, separation, and transfer properties of g-CN-U was not optimal. Based on the foregoing findings, it was concluded that the markedly improved activity of g-CN-U did not arise from their differences in light absorption intensity, energy band positions, or charge transfer properties.

The emission quenching spectrum of the suspension was then utilized to probe the photoinduced electron transfer process. As shown in Fig. 4a, the mixture displayed unvaried emission intensity when base or hydrazone was present. However, significant weakening of the emission signal occurred when hydrazone and base were both added. The strengthened interaction between g-CN-U and the deprotonated hydrazone could also be supported by the Stern-Volmer studies. As shown in Fig. 4b and Supplementary Fig. 20, the electron transfer rate between the deprotonated hydrazone and g-CN-U occurred more rapidly than other catalysts. This result could also be supported by the electrochemical study. As shown in Fig. 4c, of all the examined catalysts, g-CN-U showed the lowest oxidation overpotential, suggesting the favored kinetic due to the stronger interaction between g-CN-U and the anion intermediate.



**Fig. 3 | Mechanistic studies.** **a** Radical scavenging experiments. **b** Light on-off experiments. **c** ESR spin trapping experiments. **d** Time profile of photocatalytic

hydroamination of unsaturated  $\beta,\gamma$ -hydrazone over g-CN-U. **e** Isolation of the TEMPO-trapping product. **f** Reaction conducted in the deuterated solvent.

The adsorption and interaction of the deprotonated hydrazone over CN catalyst are carefully investigated. As revealed by the scanning electron microscopy (SEM) results (Supplementary Fig. 21), g-CN-U possessed a platelets structure with lateral dimensions of 20–60 nm, whereas the transmission electron microscope (TEM) image (Supplementary Fig. 22) exhibited one layered carbon nitride structure consisting of thin and transparent nanosheets. The Brunauer-Emmett-Teller (BET) surface area (Supplementary Fig. 23) showed g-CN-U and K-PHI showcased a much higher 56 and 76  $\text{m}^2\text{g}^{-1}$  BET surface area than g-CN-DCDA. The Barrett-Joyner-Halenda (BJH) total pore volume of g-CN-DCDA is 0.060  $\text{cm}^3/\text{g}$ , whereas g-CN-U and K-PHI possess a much larger 0.240 and 0.204  $\text{cm}^3/\text{g}$  pore volume, respectively (Supplementary Table 4). Therefore, the increased surface area of g-CN-U would benefit the mass transfer and substrate adsorption process and hence play a favorable role in the photocatalytic reaction. Zeta-potential measurement showed that K-PHI and g-CN-DCDA generally exhibited more negative potential than g-CN-U in most of the pH ranges (Fig. 4d)<sup>38</sup>, indicating a stronger interaction is more likely to be formed during g-CN-U and the deprotonated hydrazone. The CO<sub>2</sub> temperature programmed desorption (TPD) showed that the CO<sub>2</sub> desorption peak of g-CN-U owns a much lower peak intensity (Supplementary Fig. 24). The XPS spectrum of the CN samples before and after KOH treatment (denoted as g-CN-U-b, g-CN-DCDA-b, and K-PHI-b)

was compared. The N1s and C1s peaks of g-CN-U-b exhibited none of the noticeable shifts compared with g-CN-U (Supplementary Fig. 25), showing the less affected surface properties under the basic conditions. In contrast, the C-N=C, N-(C)<sub>3</sub>, and C-N-H peaks of g-CN-DCDA-b and K-PHI-b moved obviously to the lower binding energy, suggesting a higher electron density after base treatment. The relative positive surface of g-CN-U may originate from the abundant NH<sub>2</sub> groups on the large solid surface area, which could thoroughly expose to the solution and avoid large influence by the environmental conditions<sup>48</sup>. We have performed further DFT calculations to understand the relationship of NH<sub>2</sub> groups and the relative positive charged surface in the g-CN-U catalyst. g-C<sub>3</sub>N<sub>4</sub>-type carbon nitride structure is used to simulate the structure of carbon nitride without primary and secondary amino groups and melon-type carbon nitride structure is used to simulate the structure of g-CN-U photocatalyst. As shown in Supplementary Fig. 26, the g-C<sub>3</sub>N<sub>4</sub>-type carbon nitride structure exhibits a +0.1 positive charge distribution in the heptazine ring, whereas the heptazine rings of melon-type g-CN-U catalyst exhibit a much more positive charge distribution compared with that of the g-C<sub>3</sub>N<sub>4</sub> sample. This result supports that the heptazine rings in g-CN-U exhibit a positive charge distribution possibly due to the presence of rich attached NH<sub>2</sub> groups<sup>49</sup>.

Interfacial interaction of the key intermediate on the catalyst surface was investigated with <sup>1</sup>H NMR measurement. The reaction of



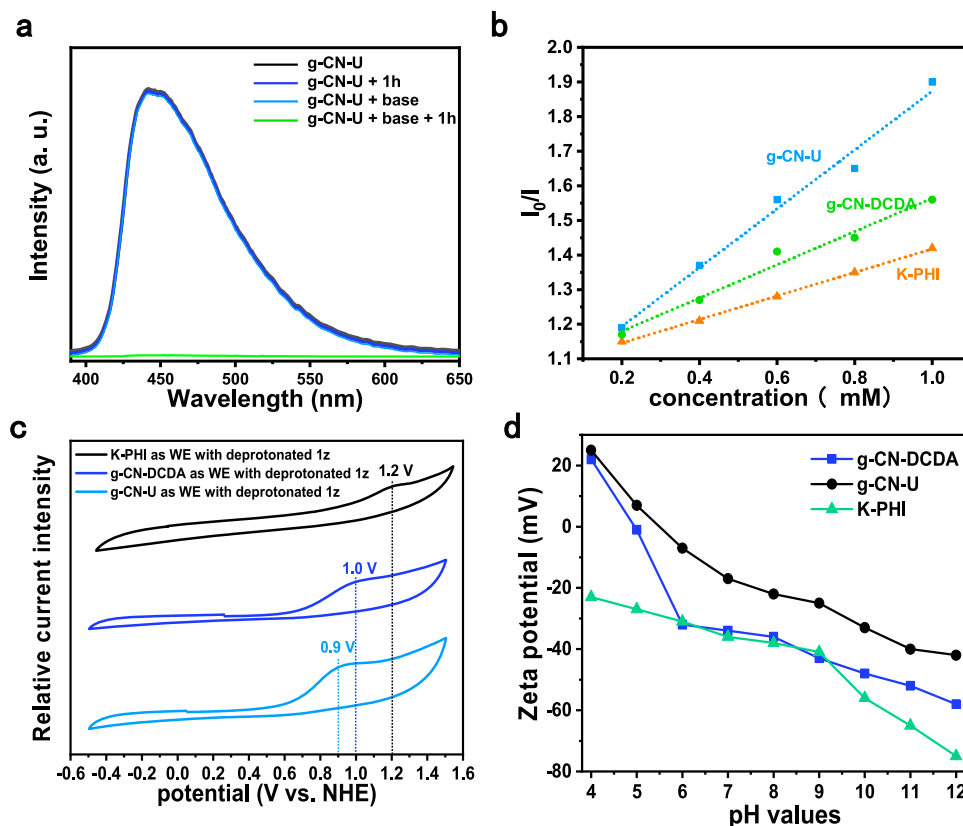


**Fig. 4 | Surface property studies.** **a** Steady-state photoluminescence spectra of g-CN-U, g-CN-U/substrate, g-CN-U/base, and g-CN-U/substrate/base in  $\text{CHCl}_3$  ( $\lambda_{\text{exc}} = 390 \text{ nm}$ ). **b** Stern-Volmer analysis of the steady-state emission intensity at 450 nm ( $\lambda_{\text{exc}} = 390 \text{ nm}$ ) with varied substrate concentration. **c** CVs obtained in a 0.1 M

tetrabutylammonium hexafluorophosphate solution containing 2 mM substrate, 2 mM base, and CN as working electrodes (WE). **d** Zeta potential of the samples under various pH values.

hydrazone and base led to the disappearance of the N-H signal at around 7.45 ppm (Supplementary Fig. 6). Addition of g-CN-DCDA to the solution led to the movement of the hydrazone proton chemical shift to the higher magnetic field, possibly resulting from the increased electron density between g-CN-DCDA negative charged surface and the nitrogen-centered anion. K-PHI could not remove the N-H proton from the hydrazone, which may originate from the stronger acidity of the NH-CN groups on the K-PHI surface. Conversely, g-CN-U led to a small proton chemical shift movement to the lower field, suggesting a decreased intermediate electron density resulting from the adsorption at the g-CN-U surface. To investigate the key role of the abundant  $\text{NH}_2$  groups and the relative positive charge distribution on the catalyst surface, for reference, H-PHI, of which the potassium cations in K-PHI are replaced by protons, was prepared by treatment of the K-PHI sample with hydrochloric acid (Supplementary Figs. 27 and 28). However, the transformation with H-PHI as the photocatalyst showed no conversion of the reaction at all. Investigation of the surface charge properties indicates that the H-PHI sample does exhibit a more positive zeta-potential at a low pH value (Supplementary Fig. 29). While due to the presence of plentiful NH-CN groups at the H-PHI surface, these acidic functional groups would quickly deprotonate under high pH value, resulting in a faster zeta potential drop rate than that of K-PHI. And the zeta potential of both samples would reach a similar value at about pH 11. This result implies that the abundant amino groups and the relative positive charged surface are both indispensable for promoting the photocatalytic activity of the transformation.

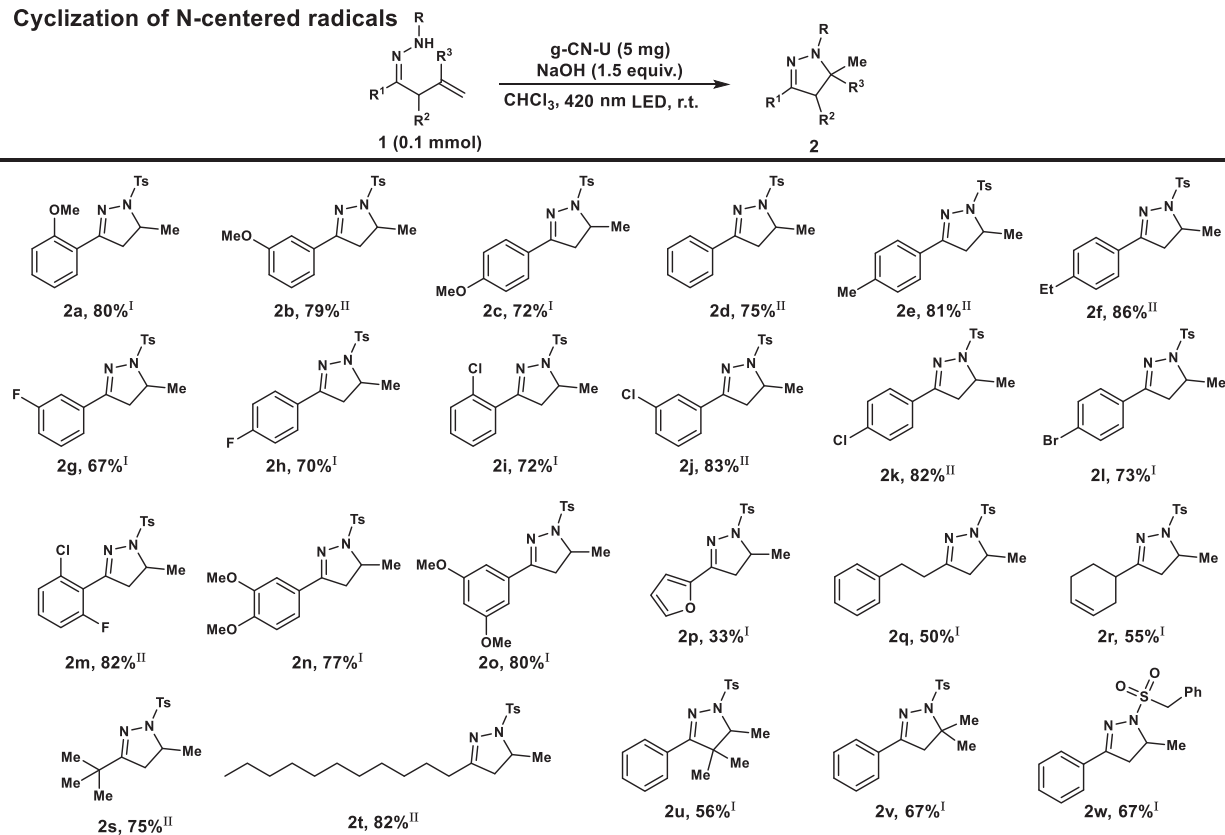
The interfacial substrate-catalyst coupling is also validated through DFT calculations on free hydrazone, deprotonated hydrazone (Supplementary Fig. 11, **Int A**), and deprotonated hydrazone adsorbed

on the melon-based structure of g-CN-U (Supplementary Fig. 30)<sup>50</sup>. As shown in Supplementary Fig. 31, the HOMO of the three systems mainly consists of N-2p orbitals. The HOMO energy of the free hydrazone molecule was calculated to be  $-5.76 \text{ eV}$  vs. vacuum. The molecular orbital position moved upward to  $-5.56 \text{ eV}$  when the base existed. The DOS diagrams for the adsorption of the deprotonated hydrazone onto the g-CN-U terminal  $-\text{NH}_2$  sites result in a further upward shift to  $-4.73 \text{ eV}$  vs. vacuum. The distance from the nitrogen atom of hydrazone to the hydrogen atom in the  $-\text{NH}_2$  group of g-CN-U is  $1.76 \text{ \AA}$  and the corresponding adsorption energy is  $-1.95 \text{ eV}$ , suggesting the formation of strong hydrogen-bonding and van der Waals interaction (Supplementary Fig. 30). Therefore, the superiority of the g-CN-U photocatalyst could be ascribed to its appropriate energy band position and large specific surface areas. More importantly, attributed to the abundant  $\text{NH}_2$  groups and positively charged surface of g-CN-U, the strong interfacial substrate-catalyst coupling greatly improved the adsorption and activation of the organic molecules. Furthermore, the upward shift HOMO position and decreased oxidation potential make the electron abstraction kinetics by the photocatalyst more energetically favorable.

### Substrate scope

The preparative scope of the reaction was investigated using a series of substituted  $\beta,\gamma$ -unsaturated hydrazones as the substrates. As illustrated in Fig. 5a, the reaction proceeded smoothly with the phenyl-derived substrates with either electron-donating (methyl, ethyl, methoxyl) or electron-withdrawing (F-, Cl-, Br-) groups at various positions (ortho, meta, para) in good yields (**2a-2l**). Bis-substituted  $\beta,\gamma$ -unsaturated hydrazone derivatives acted as competent cyclization substrates (**2m-2o**). The hydrazone containing a heterocyclic moiety

## a Cyclization of N-centered radicals



## b Other reaction types

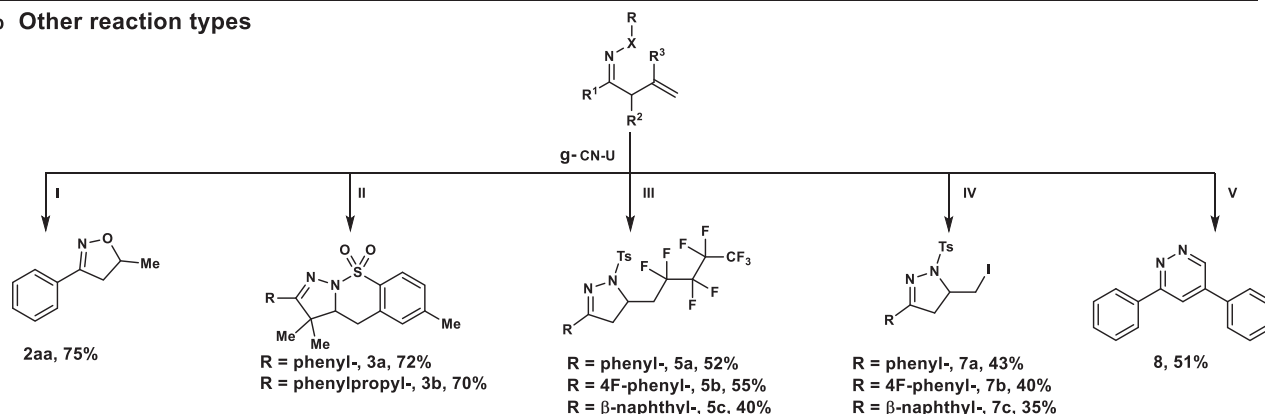


**Fig. 5 | Substrate scope.** **a** Substrate scope of  $\beta,\gamma$ -unsaturated hydrazones cyclization. Reaction conditions I (0.1 mmol), I: NaOH or II: LiOH (1.5 equiv.), g-CN-U (5 mg) in dry CHCl<sub>3</sub> (2 mL) under N<sub>2</sub> at room temperature for 8–12 h under a 3 W

420 nm LED. Isolated yields. **b** Other reaction types. I: under the 365 nm irradiation. II: [Co<sup>III</sup>(dmgH)<sub>2</sub>PyCl] as co-catalyst. III and IV: K<sub>2</sub>CO<sub>3</sub> as base for 6 h. V: TEMPO (1.0 equiv.) was added. Details in the supplementary information.

was well tolerated to deliver the product in a 33% yield. Alkyl-substituted hydrazone, including primary, secondary, and tertiary aliphatic groups, proceed smoothly to furnish the desired products (**2q–2t**). The scope could be expanded to include hydrazone with alkyl groups at the  $\alpha$ -position or terminal olefin moiety (**2u** and **2v**). N-Benzylsulfonyl-substituted hydrazones proved to be applicable to afford **2w** in 67% yield. Notably, the apparent quantum efficiency (AQE) at 420 nm for the photocatalytic production of **2a** is 7.47%, showcasing the outstanding capability of g-CN-U photocatalyst in the solar to chemical energy conversion.

As shown in Fig. 5b, the g-CN-U catalyst could promote the smooth photocatalytic cyclization of  $\beta,\gamma$ -unsaturated oxime (**2aa**). g-CN-U also proved to be a suitable photocatalyst in combination with the [Co] co-catalyst, delivering the fused tricyclic products in around 70–72% isolated yield (**3a**, **3b**)<sup>31</sup>. Beyond that, the g-CN-U exhibited satisfying activity toward radical olefin perfluoroalkylation with

concomitant  $\beta$ -functionalization (**5a–5c**)<sup>52</sup>. And this result suggested the effective generation of one reactive perfluoroalkyl radical species over g-CN-U photocatalyst, which may directly couple with the carbon-centered radical intermediate or attack the electron-rich C–C double bond of the substrate to initiate the transformation (Supplementary Fig. 32). The selectivity of the transformation was switched with iodocyclohexane as the coupling substrate (**7a–7c**), and the halocyclization product was obtained as the major product<sup>53</sup>. Finally, we were delighted to find that the corresponding biologically important pyridazines, which usually required multiple synthetic steps to prepare, could be easily afforded through a 6-endo trig cyclization of the substrate with -Ph terminal substituent in good yield (**8**)<sup>12</sup>.

## Derivatization, scalability, and catalyst recycling

The dihydropyrazole product could be effectively transformed into the biologically significant N-H pyrazole derivatives in

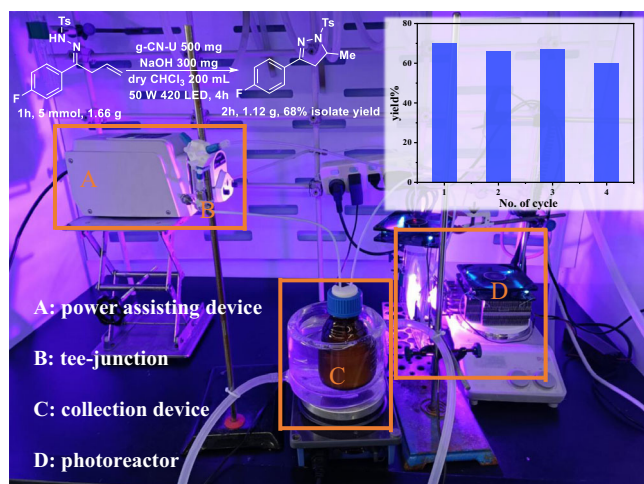


**Fig. 6 | Gram-scale reaction with a continuous-flow setup and recycling of the photocatalyst.** Reaction conditions **1h** (5 mmol, 1.66 g), NaOH (300 mg), g-CN-U (500 mg) in dry CHCl<sub>3</sub> (200 mL) under N<sub>2</sub> at room temperature for 4 h under a 50 W 420 nm LED. Isolated yields.

excellent yield (Supplementary Fig. 33). The photocatalytic process employing g-CN-U exhibited favorable scaling-up potential in terms of the reaction volume, reactant starting concentration, and stability (Fig. 6 and Supplementary Fig. 34). With the continuous flow protocol, the dihydropyrazole derivative could be obtained in 68% yield (<10% yield in batch) and the reaction period could be further reduced to only half. Furthermore, by recovering and reusing the g-CN-U photocatalyst for further characterizations and catalytic reactions, we were able to assess its stability and recyclability. The g-CN-U catalyst could be reused at least four times (Fig. 6) with only a slight attenuation of activity. There is no observed change in the crystal structure of the sample after the photocatalytic reaction, as demonstrated by the XRD, IR, and XPS characterization results (Supplementary Fig. 35–37). All the above results unambiguously confirmed the robustness and high efficiency of the metal-free g-CN-U photocatalyst for the photocatalytic cyclization process.

In conclusion, polymeric semiconductor g-CN-U is fabricated as an efficient and stable metal-free catalyst for the photocatalytic production of various pharmaceutically related heterocycles, including dihydropyrazoles, pyrazoles, tricyclic benzosultams, and pyridazines in high yields and broad substrate scope. The association between the characteristics of catalysts and their performances reveals that the interfacial coupling between catalyst and substrate is the key to the promotion of the reaction. g-CN-U with the surface complex systems could promote the highly selective oxidation of the N-H bond to nitrogen-centered radical with the synergistic combination of base and visible light, whereas g-CN-DCDA and K-PHI showed inferior activity. The formation of the chemisorbed substrate-g-CN-U surface complex is attributed to the abundant NH<sub>2</sub> groups and the relative positive charged surface on g-CN-U, which could effectively couple with the deprotonated anionic hydrazone through electrostatic attraction and H-bonding interaction. This induces a shift in the oxidation potential of the hydrazone, making it easier to remove electrons and generate the nitrogen-centered radical. This work serves as a useful reference and source of inspiration for effectively modifying carbon nitride or other metal-free photocatalysts from a kinetics-based interfacial interaction perspective. This study also demonstrates that a green and mild strategy could be achieved for the one-pot synthesis of important pharmaceutical compounds using the carbon nitride photocatalytic system.

## Methods

### Synthesis of g-CN-U

10.0 g of urea as the precursor was removed into a covered crucible and heated in a muffle furnace from room temperature to 550 °C for 2 h, followed by a further heat treatment at 550 °C for 2 h. After that, the polymer is cooled to room temperature naturally. The obtained faint yellow solid was washed with hot deionized water and ethanol three times, dried out, and collected. This sample is denoted as g-CN-U.

### Synthesis of g-CN-DCDA

10.0 g of dicyandiamide as the precursor was removed into a covered crucible and heated in a muffle furnace from room temperature to 550 °C for 2 h, followed by a further heat treatment at 550 °C for 2 h. After that, the polymer is cooled to room temperature naturally. The obtained faint yellow solid was washed with hot deionized water and ethanol three times, dried out, and collected. This sample is denoted as g-CN-DCDA.

### Synthesis of K-PHI

0.60 g of the pre-heated carbon nitride (melamine as the monomer and heated to 550 °C in a muffle furnace for 2 h and lasted for 2 h) was fully mixed with KCl (3.30 g) and LiCl (2.70 g). Then, the mixture was heated to 550 °C with 4 °C/min for 4 h under an N<sub>2</sub> atmosphere. After that, the product was washed with hot deionized water several times to remove salts and collected by filtration, followed by drying at 60 °C under vacuum. This sample is denoted as K-PHI.

### Cyclization of $\beta,\gamma$ -unsaturated hydrazone

A solution of  $\beta,\gamma$ -Unsaturated hydrazone **1** (0.1 mmol, 1 equiv.), bulk carbon nitride g-CN-U (5 mg), anhydrous sodium hydroxide, or lithium hydroxide (1.5 equiv.) in 2 mL dry chloroform were added into a Schlenk tube equipped with a stirring bar. The Schlenk tube was degassed in vacuo and purged with nitrogen five times. After finishing the freeze-pump-thaw process for several cycles, the reaction mixture was irradiated with a 3 W 420 nm LED at 25 °C for 8–12 h. After completion of the reaction monitored by TLC, the crude product was purified by short flash chromatography on silica gel (petroleum ether/ethyl acetate 12:1–8:1) to give the aim product in separation yields.

### Cyclization of $\beta,\gamma$ -unsaturated oxime

A solution of  $\beta,\gamma$ -Unsaturated oxime **1aa** (0.1 mmol, 1 equiv.), bulk carbon nitride g-CN-U (5 mg), anhydrous sodium hydroxide, or lithium hydroxide (1.5 equiv.) in 2 mL dry chloroform were added into a Schlenk tube equipped with a stirring bar. The Schlenk tube was degassed in vacuo and purged with nitrogen five times. After finishing the freeze-pump-thaw process for several cycles, the reaction mixture was irradiated with a 3 W 365 nm LED at 25 °C for 12 h. After completion of the reaction monitored by TLC, the crude product was purified by short flash chromatography on silica gel (petroleum ether/ethyl acetate 12:1–8:1) to give the product in separation yields.

### Synthesis of dihydropyrazole-fused benzosultams

A solution of **1** (0.1 mmol), g-CN-U (5.0 mg), K<sub>2</sub>CO<sub>3</sub> (27.6 mg, 0.2 mmol), [Co<sup>III</sup>(dmgH)<sub>2</sub>PyCl] (4.0 mg, 0.01 mmol) in MeCN (2.0 mL) were dissolved into a Schlenk tube. Then, the mixture was degassed via the ‘freeze-pump-thaw’ procedure (3 times) under an argon atmosphere. After that, the solution was stirred at 50 W blue LEDs (420 nm) at 80 °C for about 24 h until completion (monitored by TLC analysis). The crude product was purified by flash chromatography on silica gel (petroleum ether/ethyl acetate 10:1–3:1) directly to give the desired product **3** as a white solid.

### Data availability

The authors declare that all data generated in this study are provided in the article and the Supplementary Information file, and are also

available from the corresponding author upon request. Source data are provided with this paper.

## References

- Alex, J. M. & Kumar, R. 4,5-Dihydro-1H-pyrazole: an indispensable scaffold. *J. Enzym. Inhib. Med. Chem.* **29**, 427–442 (2014).
- Kuş, C. et al. Synthesis and antioxidant properties of novel N-methyl-1,3,4-thiadiazol-2-amine and 4-methyl-2H-1,2,4-triazole-3(4H)-thione derivatives of benzimidazole class. *Bioorg. Med. Chem.* **16**, 4294–4303 (2008).
- Wang, P. Z., Zhao, Q. Q., Xiao, W. J. & Chen, J. R. Recent advances in visible-light photoredox-catalyzed nitrogen radical cyclization. *Green. Synth. Catal.* **1**, 42–51 (2020).
- Chen, J.-R., Hu, X.-Q., Lu, L.-Q. & Xiao, W.-J. Visible light photoredox-controlled reactions of N-radicals and radical ions. *Chem. Soc. Rev.* **45**, 2044–2056 (2016).
- Xiong, T. & Zhang, Q. New amination strategies based on nitrogen-centered radical chemistry. *Chem. Soc. Rev.* **45**, 3069–3087 (2016).
- Yu, X.-Y., Zhao, Q.-Q., Chen, J., Xiao, W.-J. & Chen, J.-R. When Light Meets Nitrogen-Centered Radicals: From Reagents to Catalysts. *Acc. Chem. Res.* **53**, 1066–1083 (2020).
- Nicolaou, K. C., Zhong, Y. L. & Baran, P. S. New synthetic technology for the rapid construction of novel heterocycles-Part 2. The reaction of IBX with anilides and related compounds. *Angew. Chem. Int. Ed.* **39**, 625–628 (2000).
- Nicolaou, K. C. et al. Iodine(V) reagents in organic synthesis. Part 3. New routes to heterocyclic compounds via o-iodoxybenzoic acid-mediated cyclizations: Generality, scope & mechanism. *J. Am. Chem. Soc.* **124**, 2233–2244 (2002).
- Huynh, M. H. V. & Meyer, T. J. Proton-coupled electron transfer. *Chem. Rev.* **107**, 5004–5064 (2007).
- Gentry, E. C. & Knowles, R. R. Synthetic Applications of Proton-Coupled Electron Transfer. *Acc. Chem. Res.* **49**, 1546–1556 (2016).
- Hu, X. Q. et al. Photocatalytic Generation of N-Centered Hydrazone Radicals: A Strategy for Hydroamination of  $\beta,\gamma$ -Unsaturated Hydrazones. *Angew. Chem. Int. Ed.* **53**, 12163–12167 (2014).
- Hu, X. Q. et al. Catalytic N-radical cascade reaction of hydrazones by oxidative deprotonation electron transfer and TEMPO mediation. *Nat. Comm.* **7**, 11188 (2016).
- Wei, Q. et al. Photocatalytic Radical Trifluoromethylation/Cyclization Cascade: Synthesis of  $\text{CF}_3$ -Containing Pyrazolines and Isoxazolines. *Org. Lett.* **17**, 4464–4467 (2015).
- Margrey, K. A. & Nicewicz, D. A. General Approach to Catalytic Alkene Anti-Markovnikov Hydrofunctionalization Reactions via Acridinium Photoredox Catalysis. *Acc. Chem. Res.* **49**, 1997–2006 (2016).
- Lesieur, M., Genicot, C. & Pasau, P. Development of a Flow Photochemical Aerobic Oxidation of Benzylic C-H Bonds. *Org. Lett.* **20**, 1987–1990 (2018).
- Nikitas, N. F., Gkizis, P. L. & Kokotos, C. G. Thioxanthone: a powerful photocatalyst for organic reactions. *Org. Biomol. Chem.* **19**, 5237–5253 (2021).
- Tucker, J. W. & Stephenson, C. R. J. Shining Light on Photoredox Catalysis: Theory and Synthetic Applications. *J. Org. Chem.* **77**, 1617–1622 (2012).
- Lowry, M. S. et al. Single-layer electroluminescent devices and photoinduced hydrogen production from an ionic iridium(III) complex. *Chem. Mater.* **17**, 5712–5719 (2005).
- Yu, S. X. et al. Local spatial charge separation and proton activation induced by surface hydroxylation promoting photocatalytic hydrogen evolution of polymeric carbon nitride. *Nano Energy* **50**, 383–392 (2018).
- Xue, S. K. et al. Interfacial engineering of lattice coherency at ZnO-ZnS photocatalytic heterojunctions. *Chem. Catal.* **2**, 125–139 (2021).
- Xu, J. X. et al. & Shalom, M. Supramolecular Chemistry in Molten Sulfur: Preorganization Effects Leading to Marked Enhancement of Carbon Nitride Photoelectrochemistry. *Adv. Funct. Mater.* **25**, 6265–6271 (2015).
- Tanabe, K. & Hölderich, W. F. Industrial application of solid acid-base catalysts. *Appl. Catal. A Gen.* **181**, 399–434 (1999).
- Leow, W. R. & Chen, X. D. Surface Complexation for Photocatalytic Organic Transformations. *Bull. Chem. Soc. Jpn.* **92**, 505–510 (2019).
- Leow, W. R. et al.  $\text{Al}_2\text{O}_3$  Surface Complexation for Photocatalytic Organic Transformations. *J. Am. Chem. Soc.* **139**, 269–276 (2017).
- Dai, Y. T. et al. Efficient Solar-Driven Hydrogen Transfer by Bismuth-Based Photocatalyst with Engineered Basic Sites. *J. Am. Chem. Soc.* **140**, 16711–16719 (2018).
- Su, F. Z. et al. mpg- $\text{C}_3\text{N}_4$ -Catalyzed selective oxidation of alcohols using  $\text{O}_2$  and visible light. *J. Am. Chem. Soc.* **132**, 16299–16301 (2010).
- Maeda, K., Kuriki, R., Zhang, M. W., Wang, X. C. & Ishitani, O. The effect of the pore-wall structure of carbon nitride on photocatalytic  $\text{CO}_2$  reduction under visible light. *J. Mater. Chem. A* **2**, 15146–15151 (2014).
- Caputo, C. A. et al. Photocatalytic Hydrogen Production using Polymeric Carbon Nitride with a Hydrogenase and a Bioinspired Synthetic Ni Catalyst. *Angew. Chem. Int. Ed.* **53**, 11538–11542 (2014).
- Li, Y., Li, X., Zhang, H. W. & Xiang, Q. J. Porous graphitic carbon nitride for solar photocatalytic applications. *Nanoscale Horiz.* **5**, 765–786 (2020).
- Li, T. et al. Novel two-dimensional crystalline carbon nitrides beyond g- $\text{C}_3\text{N}_4$ : structure and applications. *J. Mater. Chem. A* **9**, 17–33 (2021).
- Yu, H. J. et al. Alkali-Assisted Synthesis of Nitrogen Deficient Graphitic Carbon Nitride with Tunable Band Structures for Efficient Visible-Light-Driven Hydrogen Evolution. *Adv. Mater.* **29**, 1605148 (2017).
- Chhabra, T., Dhingra, S., Nagaraja, C. M. & Krishnan, V. Influence of Lewis and Brønsted acidic sites on graphitic carbon nitride catalyst for aqueous phase conversion of biomass derived monosaccharides to 5-hydroxymethylfurfural. *Carbon* **183**, 984–998 (2021).
- Wang, X. L. et al. Brønsted base site engineering of graphitic carbon nitride for enhanced photocatalytic activity. *J. Mater. Chem. A* **5**, 19227–19236 (2017).
- Savateev, A., Ghosh, I., König, B. & Antonietti, M. Photoredox Catalytic Organic Transformations using Heterogeneous Carbon Nitrides. *Angew. Chem. Int. Ed.* **57**, 15936–15947 (2018).
- Nasir, M. S. et al. Recent development in graphitic carbon nitride based photocatalysis for hydrogen generation. *Appl. Catal. B Environ.* **257**, 117855 (2019).
- Dong, G. P., Zhang, Y. H., Pan, Q. W. & Qiu, J. R. A fantastic graphitic carbon nitride (g- $\text{C}_3\text{N}_4$ ) material: Electronic structure, photocatalytic and photoelectronic properties. *J. Photochem. Photobiol. C. Photochem. Rev.* **20**, 33–50 (2014).
- Latrache, M. & Hoffmann, N. Photochemical radical cyclization reactions with imines, hydrazones, oximes and related compounds. *Chem. Soc. Rev.* **50**, 7418–7435 (2021).
- Martin, D. J. et al. Highly Efficient Photocatalytic  $\text{H}_2$  Evolution from Water using Visible Light and Structure-Controlled Graphitic Carbon Nitride. *Angew. Chem. Int. Ed.* **53**, 9240–9245 (2014).
- Lin, L. H., Yu, Z. Y. & Wang, X. C. Crystalline Carbon Nitride Semiconductors for Photocatalytic Water Splitting. *Angew. Chem. Int. Ed.* **58**, 6164–6175 (2019).
- Zard, S. Z. Recent progress in the generation and use of nitrogen-centred radicals. *Chem. Soc. Rev.* **37**, 1603–1618 (2008).
- Xia, P. F. et al. Designing Defective Crystalline Carbon Nitride to Enable Selective  $\text{CO}_2$  Photoreduction in the Gas Phase. *Adv. Funct. Mater.* **29**, 1900093 (2019).



42. Lin, L. H. et al. Crystalline carbon nitride semiconductors prepared at different temperatures for photocatalytic hydrogen production. *Appl. Catal. B Environ.* **231**, 234–241 (2018).
43. Ho, J. M. et al. Chloroform as a Hydrogen Atom Donor in Barton Reductive Decarboxylation Reactions. *J. Org. Chem.* **78**, 6677–6687 (2013).
44. Malik, J. A., Madani, A., Pieber, B. & Seeberger, P. H. Evidence for Photocatalyst Involvement in Oxidative Additions of Nickel-Catalyzed Carboxylate O-Arylations. *J. Am. Chem. Soc.* **142**, 11042–11049 (2020).
45. Wayner, D. D. M., McPhee, D. J. & Griller, D. Oxidation and Reduction Potentials of Transient Free Radicals. *J. Am. Chem. Soc.* **110**, 132–137 (1988).
46. Hudgens, J. W., Johnson, R. D. III, Timonen, R. S., Seetula, J. A. & Gutman, D. Kinetics of the reaction  $\text{CCl}_3 + \text{Br}_2$  and thermochemistry of  $\text{CCl}_3$  radical and cation. *J. Phys. Chem.* **95**, 4400–4405 (1991).
47. Mazzanti, S., Kurpil, B., Pieber, B., Antonietti, M. & Savateev, A. Dichloromethylation of enones by carbon nitride photocatalysis. *Nat. Commun.* **11**, 1387 (2020).
48. Zhu, B. C., Xia, P. F., Ho, W. K. & Yu, J. G. Isoelectric point and adsorption activity of porous g- $\text{C}_3\text{N}_4$ . *Appl. Surf. Sci.* **344**, 188–195 (2015).
49. Chen, G. et al. Photopolymerization performed under dark conditions using long-stored electrons in carbon nitride. *Mater. Horiz.* **8**, 2018–2024 (2021).
50. Kang, Y. Y. et al. Selective Breaking of Hydrogen Bonds of Layered Carbon Nitride for Visible Light Photocatalysis. *Adv. Mater.* **28**, 6471–6477 (2016).
51. Zhao, Q.-Q., Hu, X.-Q., Yang, M.-N., Chen, J.-R. & Xiao, W.-J. A visible-light photocatalytic N-radical cascade of hydrazones for the synthesis of dihydropyrazole-fused benzosultams. *Chem. Commun.* **52**, 12749–12752 (2016).
52. Yu, J.-M. & Cai, C. Ambient-Light-Promoted Perfluoroalkylative Cyclization of  $\beta,\gamma$ -Unsaturated Hydrazones: Synthesis of Perfluoroalkylated Pyrazolines. *Eur. J. Org. Chem.* **2017**, 6008–6012 (2017).
53. Juliá, F., Constantin, T. & Leonori, D. Applications of Halogen-Atom Transfer (XAT) for the Generation of Carbon Radicals in Synthetic Photochemistry and Photocatalysis. *Chem. Rev.* **122**, 2292–2352 (2022).
- Fujian Province 2021L3003 (J.C.), the Chang Jiang Scholars Program of China T2016147 (X.W.), and the 111 Project D16008 (X.W.).

### Author contributions

X.W. and J.C. conceived and directed the project. J.C. and M.Y. designed the experiments. M.Y. and C.W. performed and analyzed the experiments. M.Y., J.C., R.L. and X.W. prepared the manuscript. X.Z. performed the theoretical calculation. All authors contributed to the analysis and interpretation of the data and commented on the final draft of the manuscript.

### Competing interests

The authors declare no competing interests.

### Additional information

**Supplementary information** The online version contains supplementary material available at <https://doi.org/10.1038/s41467-022-32623-3>.

**Correspondence** and requests for materials should be addressed to Jiajia Cheng or Xincheng Wang.

**Peer review information** *Nature Communications* thanks Norbert Hoffmann and the other, anonymous, reviewers for their contribution to the peer review of this work.

**Reprints and permission information** is available at <http://www.nature.com/reprints>

**Publisher's note** Springer Nature remains neutral with regard to jurisdictional claims in published maps and institutional affiliations.

**Open Access** This article is licensed under a Creative Commons Attribution 4.0 International License, which permits use, sharing, adaptation, distribution and reproduction in any medium or format, as long as you give appropriate credit to the original author(s) and the source, provide a link to the Creative Commons license, and indicate if changes were made. The images or other third party material in this article are included in the article's Creative Commons license, unless indicated otherwise in a credit line to the material. If material is not included in the article's Creative Commons license and your intended use is not permitted by statutory regulation or exceeds the permitted use, you will need to obtain permission directly from the copyright holder. To view a copy of this license, visit <http://creativecommons.org/licenses/by/4.0/>.

© The Author(s) 2022

### Acknowledgements

This work was financially supported by the National Natural Science Foundation of China 21961142019 (X.W.), 22072020 (J. C.), 22032002 (X.W.), and U1905214 (X.W.), the National Key Technologies R&D Program of China 2018YFA0209301 (X.W.), the Science Foundation of the